Secondary Ion Mass Spectrometry of Single Giant Unilamellar Vesicles Reveals Compositional Variability

Dashiel S. Grusky, Ahanjit Bhattacharya, Steven G. Boxer*

Department of Chemistry, Stanford University, Stanford, California, 94305-5012, United States

ABSTRACT: Giant unilamellar vesicles (GUVs) are a widely used model system to interrogate lipid phase behavior, study biomembrane mechanics, reconstitute membrane proteins, and provide a chassis for synthetic cells. It is generally assumed that the composition of individual GUVs is the same as the nominal stock composition, however, there may be significant compositional variability between individual GUVs. Although this compositional heterogeneity likely impacts phase behavior, the function and incorporation of membrane proteins, and the encapsulation of biochemical reactions, it has yet to be directly quantified. To assess heterogeneity, we use secondary ion mass spectrometry (SIMS) to probe the composition of individual GUVs using non-perturbing isotopic labels. Both ^{13}C- and ^{2}H-labeled lipids are incorporated into a ternary mixture, which is then used to produce GUVs via gentle hydration or electroformation. Simultaneous detection of seven different ion species via SIMS allows for the concentration of ^{13}C- and ^{2}H-labeled lipids in single GUVs to be quantified using calibration curves, which correlate ion intensity to composition. Additionally, the relative concentration of ^{13}C- and ^{2}H-labeled lipids is assessed for each GUV via the ion ratio $^{2}H^{-}/^{13}C^{-}$, which is highly sensitive to compositional differences between individual GUVs and circumvents the need for calibration using standards. Both quantification methods suggest that gentle hydration produces GUVs with greater compositional variability than those formed by electroformation. However, both gentle hydration and electroformation display compositional variability on the order of 5-15 mol percent.

Introduction

GUVs (giant unilamellar vesicles) are a commonly used model system to probe lipid phase behavior[1–4], membrane-protein interactions[5–10], and to encapsulate cellular machinery[11–14]. GUVs are an attractive model systems not only due to their large size (typically 10 to 20 μm in diameter), which allows for convenient imaging via optical microscopy[15–18], but also due to their ease of production.

GUVs are commonly produced by either gentle hydration or electroformation. Although both methods start with a lipid mixture dried as a film, for gentle hydration the film is dried onto glass, while for electroformation the film is dried onto either platinum electrodes or iridium tin oxide slides[19]. Films used for gentle hydration have either aqueous buffer or a sucrose solution added before being heated above the melting point of the lipid mixture[20–22]. Films used for electroformation are also rehydrated, typically at low ionic strength, before alternating current is applied to the film, which assists in the formation of GUVs[23–28].

Despite their widespread use, there is some evidence pointing to potential issues with GUVs as model systems. In particular, prior work has shown that electroformed GUVs composed of a ternary mixture exhibit significant variation in areas occupied by an L_d partitioning fluorescent dye.[3] Other work has shown that individual GUVs produced from the same lipid film show significant variations in their phase behavior[29,30]. Although work has been done to compare GUV formation methods in terms of their resulting unilamellarity, capacitance, shear viscosity and number of defects visible by fluorescence microscopy[31,32], compositional variability has yet to be directly examined. Quantifying this variability is critical as lipid composition is the primary variable in all GUV-based measurements. Here, we examine the compositional variability between individual GUVs using stable isotope labeling and secondary ion mass spectrometry (SIMS).

SIMS can be used to measure isotopic ratios present in a sample with high precision[33,34]. The Cameca NanoSIMS 50L functions by collisional sputtering of a freeze-dried bilayer containing isotopically labeled lipids with primary cesium ions (Cs^{+}). This process ejects secondary ions, which are then separated by a mass analyzer, allowing for up to seven individual species to be detected simultaneously. The high sensitivity and mass precision of the NanoSIMS 50L allows for compositional information of individual bilayers to be obtained[34,35]. For the experiments reported here, GUVs formed via either gentle hydration or electroformation were exposed to NanoSIMS substrates (10 nm SiO_2 coated Si) where they rupture to form supported bilayer patches whose area reflects the surface area of the parent GUV. This process is depicted in Figure 1. In parallel, continuous supported bilayers (SLBs) were formed by conventional small vesicle fusion. SIMS can then be used to examine the compositional variability of the resulting SLBs formed via different methods.

The resulting compositional variability is assessed either via external calibration curves which determine absolute concentrations of isotopically labeled lipids in an SLB or by examining the relative concentrations of two isotopically labeled lipids. This second method avoids relying on the accuracy of external standards and is not subject to potential contamination of the NanoSIMS substrate. Both methods demonstrate that patches formed from individual GUVs show considerable composition variation, and that GUVs prepared via electroformation are less variable than GUVs formed via gentle hydration. Additionally, quantification of the average concentration of cholesterol in GUVs formed via gentle hydration and electroformation suggest that GUVs formed by

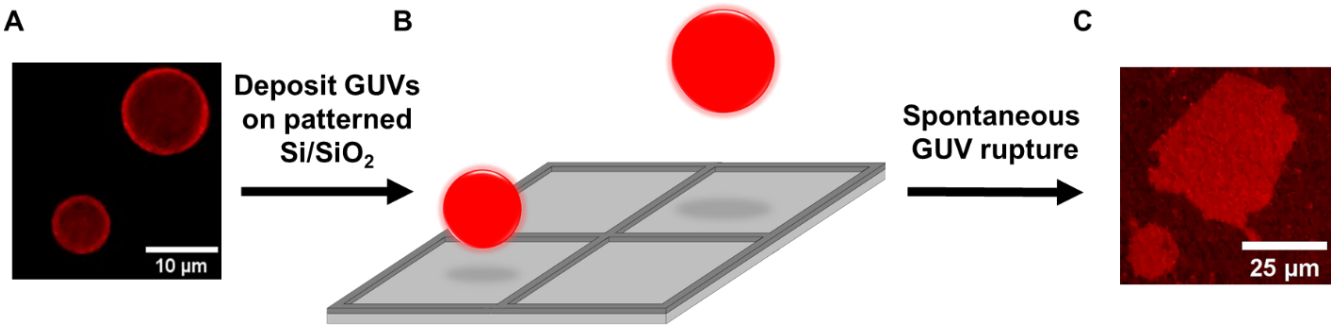

Figure 1 Experimental Design. Micron-sized giant unilamellar vesicles (GUVs) formed by gentle hydration or electroformation are deposited over patterned Si/SiO_2 substrates. GUVs spontaneously rupture to form individual GUV-derived planar supported bilayer patches that are subsequently freeze-dried and analyzed via NanoSIMS. (A) Displays epifluorescence images of POPC GUVs containing 0.1% TR-DHPE. (B) GUVs are deposited over an oxidized silicon substrate with a chrome grid and allowed to rupture. The patterning provides a visual guide for locating patches during NanoSIMS imaging. (C) Epifluorescence images of POPC GUV patches containing 0.1% TR-DHPE. Note that if small vesicles are present within the GUV these are lost or possibly deposited elsewhere upon bilayer patch formation.

electroformation have significantly less cholesterol on average than GUVs formed via gentle hydration.

Materials and Methods

All natural abundance lipids, cholesterol and $^{2}H_{31}$-POPC (1-palmitoyl-2-oleoyl-*sn*-glycero-3-phosphocholine) were purchased from Avanti Polar Lipids. $^{2}H_{7}$-cholesterol was purchased from Cayman Chemical. Texas Red 1,2-dihexadecanoyl-*sn*-glycero-3-phosphoethanolamine (TR-DHPE) was purchased from Thermo Fisher Scientific. Four inch <100> p-type silicon wafers (9.5 nm SiO_2) were purchased from Silicon Quest International and were diced to 5x5 mm to fit in the NanoSIMS sample holder. NanoSIMS substrates were patterned with a chrome grid (5nm height, 5µm width) with 25, 50 or 100 μm^2 dimensions via photolithography to facilitate correlative imaging by fluorescence microscopy. All solvents were purchased from Fisher. $^{13}C_{18}$-POPC, $^{13}C_{18}$-DSPC (1,2-distearoyl-*sn*-glycero-3-phosphocholine), and ^{15}N-POPC were synthesized as previously described[34,36]. $^{13}C_{27}$-cholesterol was isolated as previously described[37]. Structures for the labeled lipids used in this study can be seen in Figure 2.

Master Stock Solutions. Master stock solutions were prepared with the lipid mixture of interest dissolved in chloroform in high enough quantities such that multiple batches of GUVs could be produced from the same vial. Master stocks were made by first adding several hundred microliters of chloroform to a 2 mL glass vial. Lipids were then added to the vial by withdrawing the appropriate volume from a pure lipid stock solution in chloroform and then injecting the volume beneath the chloroform in the master stock vial. This ensured that each lipid remains fully dissolved within the master stock. All master stocks also contained 0.1 mol % TR-DHPE so GUV patches could be examined via fluorescence microscopy once ruptured on patterned substrates. Critically, any comparison between different methods of GUV formation was done using lipid films produced from one of these master stocks.

Gentle Hydration. Films were dried down in 2 mL glass vials from Fisher. First, 200mL of chloroform was added to a glass vial. 50nmol of lipid in chloroform was taken from a master stock and added beneath the 200mL of chloroform in the vial such that the lipid mixture remained dissolved. The glass vial was then vortexed, bath sonicated and vortexed again for 30 seconds each. The film was then dried down under a stream of argon. The vial was then placed in a desiccator overnight to remove any residual solvent. Films were then rehydrated in 0.5 mL of submicron filtered 500mM sucrose and heated to 65 ˚C, above the melting temperature of DSPC (54.4 ˚C), for 15 hours.

Electroformation. The electroformation chamber and platinum electrodes were thoroughly cleaned before lipid films were dried on the electrodes. The chamber was first bath sonicated at 56 ˚C in a mixture of 7x detergent, ethanol and deionized water in a 1:3:3 ratio. The setup was then rinsed in deionized water for 20 minutes before being further bath sonicated in deionized water and rinsed again with deionized water for another 20 minutes. The chamber was then sonicated in ethanol at room temperature. After removing the chamber from the ethanol, the setup was dried immediately and kept in a desiccator until use. Films were formed by directly spreading 66nmol of lipid taken from a master stock onto the platinum electrodes. After spreading lipids on the electrodes, the chamber was kept in a desiccator overnight to remove residual chloroform. The chamber was then sealed with clean glass slides and vacuum grease. Once sealed, the chamber was filled with 1.5mL of submicron filtered and degassed 500mM sucrose

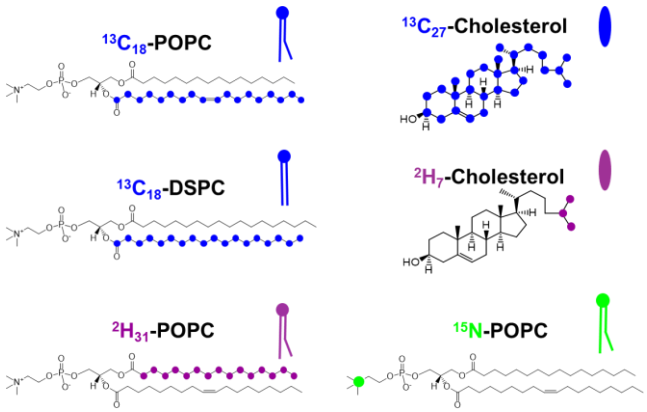

Figure 2 Labeled lipids. Isotopically labeled lipids used in this study are shown above. Color-coded circles represent locations of isotopic labels.

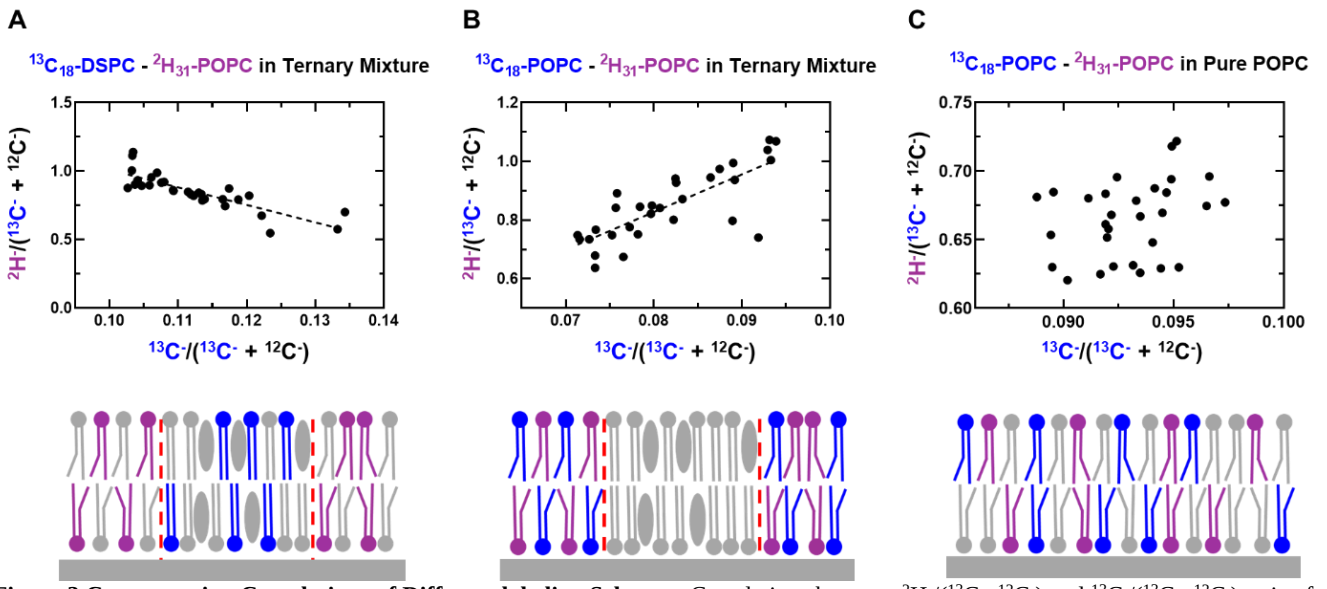

Figure 3 Concentration Correlations of Different labeling Schemes. Correlations between $^{2}H^{-}/(^{13}C^{-}+^{12}C^{-})$ and $^{13}C^{-}/(^{13}C^{-}+^{12}C^{-})$ ratios for each lipid mixture. The $^{2}H^{-}/(^{13}C^{-}+^{12}C^{-})$ ratio tracks the amount of ^{2}H-labeled lipid in the bilayer, while the $^{13}C^{-}/(^{13}C^{-}+^{12}C^{-})$ ratio tracks the amount of ^{13}C-labeled lipid in the bilayer. Cartoons below each plot depict which lipids are labeled and their location in the bilayer. Red dashed lines within these cartoons denote nanoscale separation between L_o and L_d domains (not resolvable by the 50nm lateral resolution of the NanoSIMS) (A) Correlation between $^{2}H_{31}$-POPC and $^{13}C_{18}$-DSPC ratios in the ternary mixture DSPC:$^{13}C_{18}$-DSPC:POPC:$^{2}H_{31}$-POPC:CHOL 20:20:20:20:20. (B) Correlation between $^{2}H_{31}$-POPC and $^{13}C_{18}$-POPC ratios in the ternary mixture DSPC:$^{13}C_{18}$-POPC:$^{2}H_{31}$-POPC:CHOL 40:20:20:20. (C) Absence of correlation between $^{2}H_{31}$-POPC and $^{13}C_{18}$-POPC ratios in a pure POPC mixture with composition $^{13}C_{18}$-POPC:$^{2}H_{31}$-POPC:POPC 20:20:60.

before being heated to 65 ˚C. GUVs were electroformed at 10Hz, 3V (peak to peak) for 2 hours and then at 1 Hz, 3V for another 30 minutes.

Vesicle extrusion. Glass test tubes were filled with 200mL of chloroform. 28nmol of lipid from a master stock was then injected beneath chloroform in the test tube. Lipid films were then dried down under argon onto the test tube sides before being desiccated overnight. Films were then resuspended in 1x phosphate buffered saline (137mM NaCl, 2.7 mM KCl, 8mM $NaPO_4$, pH 7.2, submicron filtered) and vortexed for 1 minute. The buffer with the resuspended lipids was then passed through a membrane with 100nm pore size 61 times while being heated to 65 ˚C to form SUVs (small unilamellar vesicles).

NanoSIMS sample preparation. GUVs were ruptured onto silicon substrates to form SLB patches after being allowed to briefly cool to room temperature. Silicon substrates were plasma cleaned for 10 minutes after which they were submerged in phosphate buffer (240 mM NaCl, 10 mM NaH_2PO_4 at pH 7.4). Then GUVs were deposited over the submerged substrates and allowed to incubate until approximately 10-15% of the surface was covered in SLB patches. GUV deposition was observed with a Nikon Eclipse 80i epifluorescence microscope equipped with an Andor Clara camera. The substrate and bilayers were then extensively washed with MilliQ water. Although GUVs, particularly those formed via gentle hydration, can be multivesicular, upon GUV rupture to form an SLB patch, the internal vesicles are liberated and rinsed away. Cleaned substrates were flash frozen in liquid nitrogen and then subjected to low pressure for at least 12 hours to sublimate any vitreous ice.

To form continuous bilayers on NanoSIMS substrates, 100nm vesicles were incubated over plasma cleaned substrates for 1 minute before being washed extensively with MilliQ water. Continuous bilayers on substrates were found to be more susceptible to de-wetting during flash freezing, so substrates with continuous bilayers were removed from MilliQ water with the bilayer facing upside-down. This ensured that a drop of water remained in contact with the bilayer at all times before the substrate was flash-frozen in liquid nitrogen. Once frozen, substrates were subjected to low pressure using the same method as GUV patch samples.

Lipid monolayers were formed using a KSV NIMA KN 2002 (Biolin Scientific, Stockholm, Sweden) Langmuir trough (273 cm^2). Whatmann filter paper was used as a Wilhelmy plate to monitor surface pressure. Lipid mixtures dissolved in chloroform were spread on water (>18 MΩ from Milli-Q system) within the clean trough using a glass syringe. The chloroform was left to evaporate for 10 minutes and the barriers were compressed at 10 mm/min until the surface pressure reached 32 mN/m. Plasma cleaned NanoSIMS substrates were glued to a glass slide and pulled through the air-water interface at a rate of 1 mm/min while the surface pressure was maintained at 32 mN/m. Lipid monolayers were not subjected to freeze-drying, as unlike SLBs, lipid monolayers are stable in air. Both lipid monolayers and freeze-dried lipid bilayers were stored in a desiccator when not being analyzed via NanoSIMS.

NanoSIMS Analysis. Analysis was performed on the Cameca NanoSIMS 50L at Stanford University. Correlative fluorescence imaging helped facilitate the selection of bilayer patches such that debris on the substrate surface was avoided. Bilayer patches were imaged with a 2pA $^{133}Cs^{+}$ primary beam. Ten 25x25 micron scans (256x256 pixels, 1ms dwell time) were collected, which is enough to remove all of the deposited material on the surface. Secondary ion detectors were set to $^{2}H^{-}$, $^{12}C^{-}$, $^{13}C^{-}$, $^{12}C_2H^{-}$,$^{12}C_2{}^{2}H^{-}$, $^{13}C_2H^{-}$, and $^{13}C_2{}^{2}H^{-}$ for samples containing ^{2}H- or ^{13}C-labeled lipids of cholesterol. If ^{15}N-

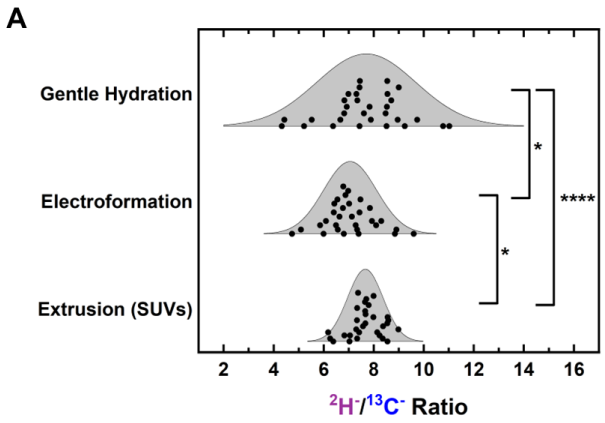

B

Method	$^{2}H^{-}/^{13}C^{-}$ Standard Deviation
Gentle Hydration	1.593
Electroformation	1.059
Extrusion (SUVs)	0.7101

Figure 4 Measured $^{2}H^{-}/^{13}C^{-}$ ratios for different methods. GUV patches formed by gentle hydration and electroformation, were compared to continuous bilayers formed from SUVs via their $^{2}H^{-}/^{13}C^{-}$ ratios. All samples were produced from a master stock with nominal composition DSPC:$^{13}C_{18}$-DSPC:POPC:$^{2}H_{31}$-POPC:CHOL 20:20:20:20:20. (A) Displays the $^{2}H^{-}/^{13}C^{-}$ ratio distributions for each preparation method. Significance was determined via F-test. For this and subsequent plots, each point represents a measurement made on a single GUV patch or corral containing an SLB. Thirty bilayers were examined for each sample. For this and all subsequent plots, * $p \leq 0.05$, ** $p \leq 0.01$, *** $p \leq 0.001$, **** $p \leq 0.0001$. The displayed curves are normal distributions calculated using the standard deviation and average from the GUV patch measurements. (B) Calculated standard deviations of the $^{2}H^{-}/^{13}C^{-}$ ratio for each preparation method.

labeled POPC was contained within SLB patches, secondary ion detectors were set to $^{2}H^{-}$, $^{12}C^{-}$, $^{13}C^{-}$, $^{12}C_{2}H^{-}$,$^{12}C^{14}N^{-}$, $^{13}C^{15}N^{-}$, and $^{13}C_{2}{}^{2}H^{-}$. Standard samples (the calibration curves described below) were regularly analyzed to ensure that isotope ratios were reproducible from session to session.

Data Analysis. Images were analyzed using ImageJ (National Institutes of Health, USA) with the OpenMIMS plugin (National Resource for Mass Spectrometry, Harvard University USA). Planes were summed and regions of interest were manually selected in order to exclude any debris on the sample. Total counts within each region of interest were determined via the "Tomography" tab. These counts were then used to determine the ratios of interest (typically $^{2}H^{-}/^{13}C^{-}$, $^{13}C^{-}/(^{13}C^{-} + {}^{12}C^{-})$ and $^{2}H^{-}/(^{13}C^{-} + {}^{12}C^{-})$). Calculating these ratios allows for the size of the analyzed patches to be accounted for and allows for further quantification via external calibration standards.

Calibration Standards. Concentration calibration standards were made from lipid mixtures dissolved in chloroform containing a known mol % of labeled lipid. Calibration standards used to quantify labeled lipid concentrations in ternary SLBs contained 20 mol % cholesterol, as this is present in the ternary mixture. Calibration curves without cholesterol were also prepared so that labeled lipids concentrations in mixtures without cholesterol could quantified. The prepared lipid mixtures dissolved in chloroform were spread on plasma cleaned NanoSIMS substrates. The chloroform was then allowed to evaporate to form a lipid film. Concentration calibration standards were kept in a desiccator until use.

Results and Discussion

Comparing GUV Preparation Methods via Double-Labeling. First, we assessed the variability in relative concentrations of labeled lipids for different GUV preparation methods. Although direct concentration quantification via external calibration curves can give estimates of the concentration of a labeled species, this method is subject to inaccuracies. These experiments can be skewed by surface contamination and are heavily reliant on the accuracy of the calibration standards. In order to avoid these issues, and inspired by prior work[38], initial experiments examined the relative change in ion counts from patch to patch resulting from two lipids with different isotopic labels. This was done with a POPC:DSPC:CHOL 40:40:20 mixture. This mixture was chosen as GUV patches with this composition do not display macroscopic phase separation between lipid components within the 50 nm lateral resolution of the NanoSIMS primary ion beam (Figure S1; there is nanoscale separation present in these SLB patches which can be detected by ion-recombination[36]). This mixture is also well-studied in GUVs and GUV patches[4,36,39].

In order to determine which pair of labeled lipids is most sensitive to relative changes in concentration, two ternary samples, one with the composition $^{13}C_{18}$-DSPC:POPC:$^{2}H_{31}$-POPC:CHOL 20:20:20:20:20 and the other with the composition DSPC:$^{13}C_{18}$-POPC:$^{2}H_{31}$-POPC:CHOL 40:20:20:20 were prepared. Additionally, a sample with the composition $^{2}H_{31}$-POPC:$^{13}C_{18}$-POPC:POPC 20:20:60 was also prepared (samples with this composition are denoted as pure POPC). $^{13}C^{-}/(^{13}C^{-} + {}^{12}C^{-})$ and $^{2}H^{-}/(^{13}C^{-} + {}^{12}C^{-})$ ratios were then measured for 30 GUV patches formed via gentle hydration for all three samples.

Figure 3 shows the correlation between the $^{2}H^{-}/(^{13}C^{-} + {}^{12}C^{-})$ and $^{13}C^{-}/(^{13}C^{-} + {}^{12}C^{-})$ ratio for each labeling scheme. The $^{2}H^{-}/(^{13}C^{-}+{}^{12}C^{-})$ ratio tracks the amount of ^{2}H-labeled lipid in the bilayer, while the $^{13}C^{-}/(^{13}C^{-} + {}^{12}C^{-})$ ratio tracks the amount of ^{13}C-labeled lipid in the bilayer. Figure 3 demonstrates that the correlation between the ratios is a function of both the location of the isotopic label and the overall composition of the bilayer. The ternary mixture containing both $^{2}H_{31}$-POPC and $^{13}C_{18}$-POPC shows a positive correlation between lipid concentrations. Conversely, the ternary mixture containing $^{2}H_{31}$-POPC and $^{13}C_{18}$-DSPC displays a clear negative correlation between the concentrations of the two components. These trends can be attributed to preferential interactions between $^{13}C_{18}$-POPC and $^{2}H_{31}$-POPC and unfavorable interactions between $^{13}C_{18}$-DSPC and $^{2}H_{31}$-POPC within ternary bilayers. These interactions are depicted schematically in the cartoons shown in Figure 3.

As shown in Figure 3C, pure POPC SLBs containing $^{2}H_{31}$-POPC and $^{13}C_{18}$-POPC did not show any clear correlation in

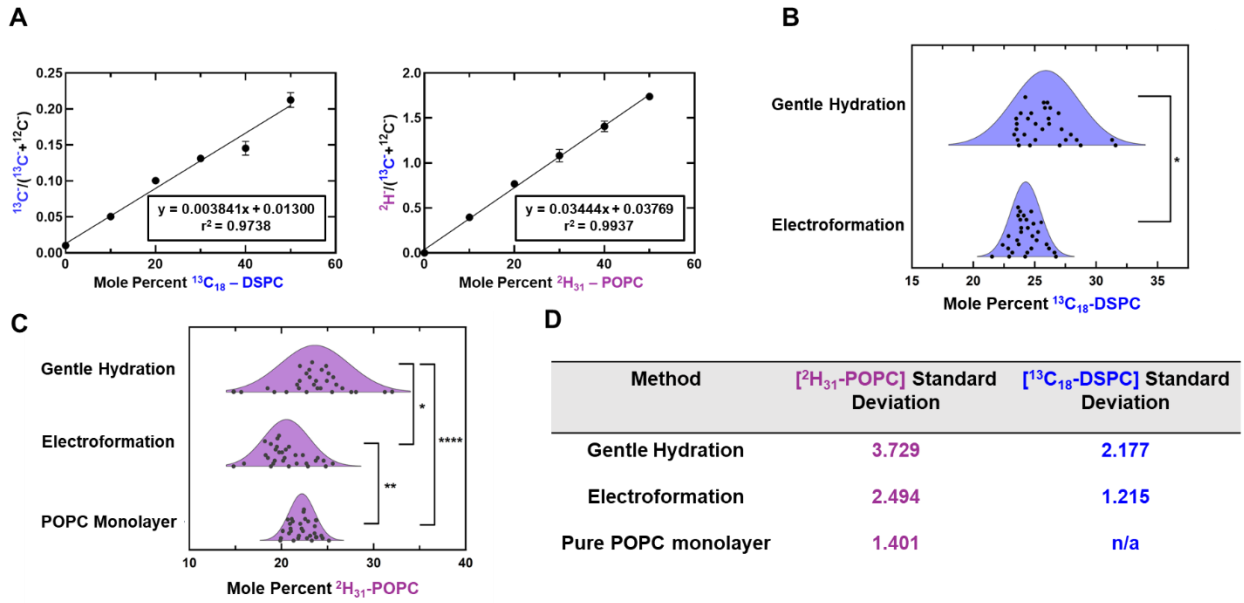

Method	[$^{2}H_{31}$-POPC] Standard Deviation	[$^{13}C_{18}$-DSPC] Standard Deviation
Gentle Hydration	3.729	2.177
Electroformation	2.494	1.215
Pure POPC monolayer	1.401	n/a

Figure 5 Concentration quantification of GUV patches and monolayers. (A) Representative calibration curves for $^{13}C_{18}$-DSPC and $^{2}H_{31}$-POPC. (B) Displays the calculated $^{13}C_{18}$-DSPC and concentration distributions for GUV patches formed by gentle hydration and electroformation. All GUVs were formed using a ternary mixture with nominal composition DSPC:$^{13}C_{18}$-DSPC:POPC:$^{2}H_{31}$-POPC:CHOL 20:20:20:20:20. Gentle hydration $^{13}C_{18}$-DSPC concentrations are significantly different as determined by F-test. (C) Displays the calculated $^{2}H_{31}$-POPC concentrations distributions for GUV patches formed by gentle hydration and electroformation. These concentration distributions are compared to $^{2}H_{31}$-POPC concentrations measured in a monolayer composed of POPC with 20 mol % $^{2}H_{31}$-POPC. (D) Calculated standard deviations for each concentration distribution.

concentration between the differently labeled lipids. Since the $^{2}H_{31}$-POPC, $^{13}C_{18}$-POPC and natural abundance POPC within the pure POPC mixture only differ from each other in terms of isotopic labeling, when the concentration of one labeled component is higher in a GUV, whether the concentration of a labeled or natural abundance POPC is lower is essentially random.

Based on the results from Figure 3, a ternary mixture containing $^{13}C_{18}$-DSPC and $^{2}H_{31}$-POPC is expected to be the most sensitive to relative concentration changes between the two labeled lipids, as the concentrations of these two components are anti-correlated. Therefore, this mixture was used to study the compositional variability of GUVs formed by electroformation or gentle hydration.

GUVs with this composition were generated from the same master stock either by gentle hydration or electroformation. The same master stock was also used to generate 100nm SUVs which were then ruptured onto NanoSIMS substrates to form continuous bilayers within the corrals of the patterned NanoSIMS substrate. Since these continuous bilayers are formed from hundreds of SUVs, the relative concentrations of $^{13}C_{18}$-DSPC and $^{2}H_{31}$-POPC should be more consistent than in SLB patches formed from the rupture of a single GUV. The measured $^{2}H^{-}/^{13}C^{-}$ ratio for 30 individual bilayer patches or 30 corrals containing continuous bilayers is shown in Figure 4. Based on the measured ratios, gentle hydration has the highest variation in relative concentration when compared to electroformation, with significance determined via F-test (the normality of each distribution assessed by F-test is further discussed in section 2 of the supporting information). Continuous bilayers formed from SUVs have the lowest variability. Replicate samples produced from films dried down from the same master stock also suggest that electroformation is more consistent than gentle hydration (Figure S4).

Absolute Concentration Variability. Although measuring the $^{2}H^{-}/^{13}C^{-}$ ratio is useful for comparing the variability in different methods while avoiding concerns regarding surface contamination and calibration accuracy (further discussed in section 4 of the supporting information), quantification of absolute concentration is useful for determining how much the mol % of a particular lipid varies from GUV to GUV. Therefore, external calibration curves, such as those shown in Figure 5A, were used to relate quantitative ion ratios to labeled lipid concentration. This allowed for the concentration of each labeled species within one GUV patch to be determined. This analysis was performed for the GUV samples discussed in Figure 4.

As shown in Figure 5B and C, GUV patches produced via electroformation showed consistently less variability in both $^{13}C_{18}$-DSPC and $^{2}H_{31}$-POPC concentration than those formed via gentle hydration. To determine the lower bound on variability (i.e., how much of the variation in concentration measurements is due to instrument noise and surface contamination) a monolayer with overall composition $^{2}H_{31}$-POPC:$^{13}C_{18}$-POPC:POPC 20:20:60 (pure POPC composition) was formed on a NanoSIMS substrate and compared to both GUV samples. Since a monolayer should be compositionally homogenous across the substrate surface, this measurement can be used to approximate how much of the variability is due to the experimental method. As seen in Figure 5C, pure POPC monolayers demonstrated consistently less variability in $^{2}H_{31}$-POPC concentrations than that of GUVs formed via electroformation or gentle hydration. However, these monolayers cannot be compared via the $^{2}H^{-}/^{13}C^{-}$ ratio as was done in Figure 4, because the correlation between $^{2}H_{31}$-POPC and $^{13}C_{18}$-POPC concentrations in pure POPC is dramatically different from the correlation between $^{2}H_{31}$-POPC and $^{13}C_{18}$-DSPC in ternary mixtures (Figure 3). Additionally, ternary

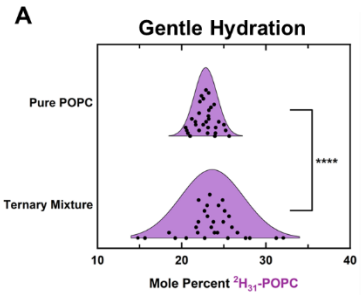

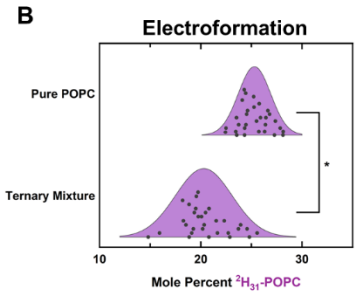

C

Method	[$^{2}H_{31}$-POPC] Standard Deviation	
	Pure POPC	Ternary Mixture
Gentle Hydration	1.350	3.729
Electroformation	1.598	2.494

Figure 6 Pure and ternary mixture concentration variability. $^{2}H_{31}$-POPC concentrations of individual GUV patches composed with pure POPC ($^{13}C_{18}$-POPC:$^{2}H_{31}$-POPC:POPC 20:20:60) or ternary ($^{13}C_{18}$-DSPC:POPC:$^{2}H_{31}$-POPC:CHOL 20:20:20:20:20) compositions were compared. Both pure POPC and ternary GUVs were formed by either electroformation (A) or gentle hydration (B). For both methods, the patches composed of pure POPC display significantly less $^{2}H_{31}$-POPC concentration variability than ternary mixtures formed using the same method. (C) Displays the calculated standard deviations for each sample.

monolayers formed from the ternary master stock containing $^{2}H_{31}$-POPC and $^{13}C_{18}$-DSPC display macroscale separation (Figure S6) and are therefore not comparable to the GUV samples, as is further discussed in section 5 of the supporting information. Therefore, monolayers can only be compared to GUV samples via absolute concentrations. Additional analysis suggests that the size of the region selected for quantification within the 25x25 μm analysis region does not significantly impact the distributions shown in Figures 4 and 5 (further discussed in section 6 of the supporting information). Therefore, the intrinsic signal to noise of a single patch is unlikely to substantially impact the GUV variability observed for different formation methods.

Sources of Variability. In order to further explore sources of the observed GUV variability, GUVs with pure POPC composition ($^{2}H_{31}$-POPC:$^{13}C_{18}$-POPC:POPC 20:20:60) were formed by either gentle hydration or electroformation. 30 GUV patches with this composition were analyzed for each method, and their absolute concentrations determined via external calibration curves. In Figure 6, the calculated $^{2}H_{31}$-POPC concentrations in the pure POPC samples are compared to the $^{2}H_{31}$-POPC concentrations in the previously discussed ternary mixture. Ternary GUV patches formed either by electroformation or gentle hydration displayed significantly more variability in $^{2}H_{31}$-POPC concentrations relative to pure POPC patches formed by the same method. This lower variability for the pure POPC GUVs can also be seen for the $^{13}C_{18}$-labeled lipids (Figure S9). These results suggest that more complex lipid compositions lead to considerably more compositional variability. It also suggests that the observed compositional variability is not only due to residual contamination of either the platinum electrodes used for electroformation or glass vials used for gentle hydration. If these surfaces had significant contamination, pure POPC patches would have compositional variability comparable to ternary patches. Comparison of $^{2}H_{31}$-POPC concentration variability between pure POPC patches formed via either electroformation or gentle hydration did not show a significant difference in compositional variability (Figure S10). This suggests that the higher variability observed in GUV patches formed via gentle hydration (Figures 4 and 5) is not due to higher residual contamination on glass vials relative to the platinum electrodes, but rather results from the complexity of the ternary mixture and the method of GUV formation. Additionally, the average $^{2}H^{-}$, $^{12}C^{-}$ and $^{13}C^{-}$ counts were compared between regions of interest with and without bilayer to gauge the level of contamination on the substrate surface (Figure S11). Regions of interest containing bilayer showed considerably higher signal on all detectors than regions of interest on exposed substrate. Further analysis was also performed to correct the observed variabilities in ternary GUV patches for noise due to sample preparation and analysis (discussed in section 10 of the supporting information).

To further examine potential sources of variability, lipid films from the master stock containing $^{13}C_{18}$-DSPC and $^{2}H_{31}$-POPC were dried down directly on NanoSIMS substrates and imaged. No significant separation within the 50nm lateral resolution of the NanoSIMS was observed between $^{13}C_{18}$-DSPC and $^{2}H_{31}$-POPC within the film (Figure S13). However, atomic recombination experiments demonstrated that there is nanoscale separation between POPC and DSPC (Figure S14). Although this does not demonstrate that this nanoscale separation is responsible for the observed GUV compositional variability, it does suggest that there are preferential interactions within lipid films. These interactions may contribute to lipid sorting while GUVs are being formed. Additional experiments also suggest that the size of the GUV patch analyzed is not correlated with the either $^{13}C_{18}$-DSPC or $^{2}H_{31}$-POPC concentrations (section 12 of the supporting information). Furthermore, additional data suggest that two different GUVs typically do not rupture to form one patch (section 13 of the supporting information). This suggests that most patches are the product of a single GUV and that minimal compositional averaging between GUVs occurs.

Quantifying Cholesterol Concentrations. Cholesterol concentration was also examined in GUV patches. Unlike phospholipids, Cholesterol localized significantly to the edges of GUV patches formed by either electroformation or gentle hydration as seen in Figure 7A and Figure S18. This makes quantification of cholesterol variability in GUVs significantly more challenging as the relative ratio of edge to center within the analyzed region needs to be considered as well as how the overall concentration of cholesterol in a patch may affect its partitioning between the edge and center. As a result, the variability in cholesterol concentration from GUV to GUV was not assessed. Instead, the average cholesterol concentration was determined for different GUV formation methods. Ternary GUV patches were formed via gentle hydration and electroformation using a master stock with nominal composition DSPC:POPC:$^{2}H_{31}$-POPC:$^{13}C_{27}$-CHOL 40:20:20:20. The average concentration was then calculated either including or excluding the cholesterol-rich edges.

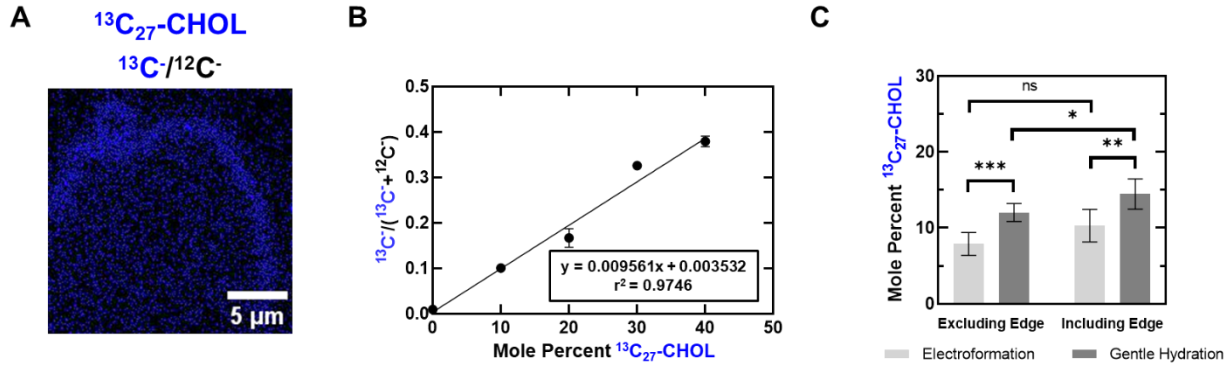

Figure 7 Cholesterol concentration differences between electroformation and gentle hydration. GUVs were formed via electroformation or gentle hydration from a master stock with nominal composition DSPC:POPC:$^{2}H_{31}$-POPC:$^{13}C_{27}$-CHOL 40:20:20:20. (A) NanoSIMS image of a GUV patch formed via electroformation, which shows significant localization of $^{13}C_{27}$-CHOL to the edge of the GUV patch. (B) $^{13}C_{27}$-CHOL calibration curve. (C) Comparison $^{13}C_{27}$-CHOL concentration in GUV patches formed via gentle hydration or electroformation. Error bars represent 95% confidence intervals. Comparisons were conducted either excluding the edge of the bilayer patch or including the edge of the bilayer patch. Regardless of the analysis method, electroformed GUVs contained less cholesterol on average.

Regardless of the analysis method used, the average concentration of cholesterol was lower in electroformed GUV patches, as can be seen in Figure 7C. The average $^{2}H_{31}$-POPC concentration was the same between the two methods regardless of the analysis method (Figure S19). Average cholesterol concentration was also examined in GUV patches where all three components are isotopically labeled (Figure S18). These experiments also demonstrate lower average cholesterol concentrations in electroformed GUVs.

Although there appears to be cholesterol partitioning to the edge of bilayer patches, the increase in cholesterol concentration when the edge is included in the analysis relative to when it is excluded appears to be moderate. There is only a statistically significant difference between the analysis methods ($p = 0.0316$) with the GUVs formed via gentle hydration (Figure 7C). Replicate samples (Figure S20) do not reproduce this difference between the analysis methods.

The source of the difference in cholesterol concentrations between GUVs formed by electroformation and those formed by gentle hydration may be a result of the alternative current applied during electroformation. While the phospholipids present in the ternary mixture are zwitterionic and potentially more affected by the alternating current applied during electroformation, cholesterol is neutral, and therefore may be less responsive to the applied current. This would result in lower incorporation into electroformed GUVs. However, the experiments performed here cannot provide a definitive explanation or mechanism for the difference in cholesterol concentrations between the two methods.

Conclusions

GUVs are a widely used model system for probing lipid-protein and lipid-lipid[40,41] interactions. Despite the widespread use of GUVs, little work has been done to probe GUV-to-GUV compositional variation. This is likely due to the lack of methods to accurately assess the concentration of a given lipid within a single GUV. The Cameca NanoSIMS 50L allows for high-precision determination of the concentration of individual lipid species via non-perturbative stable isotope labeling.

Here we demonstrate that significant variability is present in GUVs composed of a ternary DSPC:POPC:CHOL mixture. It is shown that GUVs formed via electroformation have considerably less compositional variability than those formed via gentle hydration. This is true regardless of whether the relative change in concentration between two labeled species is calculated or if the variability in absolute concentration is determined via external calibration curves. Although the mechanism behind the lower variability seen in electroformed GUVs is unclear, it is clear that ternary mixtures are far more variable than pure mixtures and that preferential interactions between certain lipids are present in the films used to form ternary GUVs.

Although the variability in cholesterol concentration is not examined here, the average concentration of labeled cholesterol was compared between different methods. This demonstrated that electroformed GUVs have a lower average cholesterol concentration. Additionally, it is worth noting that other potential disadvantages have been reported with electroformation that are not discussed here[42]. Therefore, while electroformation may yield more compositionally uniform GUVs, there are downsides to the method that need to be considered.

ASSOCIATED CONTENT

The supporting information is available free of charge via the Internet at http://pubs.acs.org.

Choice of lipid mixture; Normality Verification for F-tests; Replicate Electroformation and Gentle Hydration Samples; Verification of Absolute Calibration Accuracy; Ternary Monolayers; Effect of Analysis Area on Concentration Distributions; ^{13}C-labeled Lipid comparisons in Pure and Ternary Mixtures; Comparison of Pure POPC Mixtures with different Methods; Detector Counts on Bilayer and Exposed Substrate; Correcting Ternary GUV Compositional Variability; Nanoscale Heterogeneity in Lipid Films; Relation between GUV Patch Size and $^{13}C_{18}$-DSPC and $^{2}H_{31}$-POPC Concentrations; Assessing the Extent of GUV Mixing during Patch Formation; Tracking Cholesterol Concentration in Triply Labeled Bilayers; Assessing Average $^{2}H_{31}$-POPC Concentration in $^{13}C_{27}$-CHOL Containing Patches

AUTHOR INFORMATION

Corresponding Author

* sboxer@stanford.edu

Author Contributions

D. S. G. designed experiments, performed experiments, analyzed data, and wrote the paper. A. B. provided helpful discussion. S. G. B. designed experiments and co-wrote the paper.

Funding Sources

This work was supported by grants from the NSF (MCB-1915727) and NIH (R35GM118044) to S.G.B. The Cameca NanoSIMS 50L at the Stanford Nano Shared Facilities (SNSF) is supported by the National Science Foundation (ECCS-2026822).

ACKNOWLEDGMENT

We thank Christie Jilly-Rehak and Matthew Mills at the Stanford Nanocharacterization Laboratory for instrument support on the NanoSIMS 50L.

REFERENCES

(1) Heberle, F. A.; Wu, J.; Goh, S. L.; Petruzielo, R. S.; Feigenson, G. W. Comparison of Three Ternary Lipid Bilayer Mixtures: FRET and ESR Reveal Nanodomains. *Biophys. J.* **2010**, *99* (10), 3309–3318. https://doi.org/10.1016/j.bpj.2010.09.064.

(2) Veatch, S. L.; Keller, S. L. Miscibility Phase Diagrams of Giant Vesicles Containing Sphingomyelin. *Phys. Rev. Lett.* **2005**, *94* (14), 148101. https://doi.org/10.1103/PhysRevLett.94.148101.

(3) Bezlyepkina, N.; Gracià, R. S.; Shchelokovskyy, P.; Lipowsky, R.; Dimova, R. Phase Diagram and Tie-Line Determination for the Ternary Mixture DOPC/ESM/Cholesterol. *Biophys. J.* **2013**, *104* (7), 1456–1464. https://doi.org/10.1016/j.bpj.2013.02.024.

(4) Konyakhina, T. M.; Wu, J.; Mastroianni, J. D.; Heberle, F. A.; Feigenson, G. W. Phase Diagram of a 4-Component Lipid Mixture: DSPC/DOPC/POPC/Chol. *Biochim. Biophys. Acta BBA - Biomembr.* **2013**, *1828* (9), 2204–2214. https://doi.org/10.1016/j.bbamem.2013.05.020.

(5) Jørgensen, I. L.; Kemmer, G. C.; Pomorski, T. G. Membrane Protein Reconstitution into Giant Unilamellar Vesicles: A Review on Current Techniques. *Eur. Biophys. J.* **2017**, *46* (2), 103–119. https://doi.org/10.1007/s00249-016-1155-9.

(6) Shi, Z.; Sachs, J. N.; Rhoades, E.; Baumgart, T. Biophysics of α-Synuclein Induced Membrane Remodelling. *Phys. Chem. Chem. Phys.* **2015**, *17* (24), 15561–15568. https://doi.org/10.1039/C4CP05883F.

(7) Doeven, M. K.; Folgering, J. H. A.; Krasnikov, V.; Geertsma, E. R.; van den Bogaart, G.; Poolman, B. Distribution, Lateral Mobility and Function of Membrane Proteins Incorporated into Giant Unilamellar Vesicles. *Biophys. J.* **2005**, *88* (2), 1134–1142. https://doi.org/10.1529/biophysj.104.053413.

(8) Islam, Md. Z.; Ariyama, H.; Alam, J. Md.; Yamazaki, M. Entry of Cell-Penetrating Peptide Transportan 10 into a Single Vesicle by Translocating Across Lipid Membrane and Its Induced Pores. *Biochemistry* **2014**, *53* (2), 386–396. https://doi.org/10.1021/bi401406p.

(9) Aimon, S.; Callan-Jones, A.; Berthaud, A.; Pinot, M.; Toombes, G. E. S.; Bassereau, P. Membrane Shape Modulates Transmembrane Protein Distribution. *Dev. Cell* **2014**, *28* (2), 212–218. https://doi.org/10.1016/j.devcel.2013.12.012.

(10) Garten, M.; Aimon, S.; Bassereau, P.; Toombes, G. E. S. Reconstitution of a Transmembrane Protein, the Voltage-Gated Ion Channel, KvAP, into Giant Unilamellar Vesicles for Microscopy and Patch Clamp Studies. *J. Vis. Exp.* **2015**, No. 95, 52281. https://doi.org/10.3791/52281.

(11) Göpfrich, K.; Haller, B.; Staufer, O.; Dreher, Y.; Mersdorf, U.; Platzman, I.; Spatz, J. P. One-Pot Assembly of Complex Giant Unilamellar Vesicle-Based Synthetic Cells. *ACS Synth. Biol.* **2019**, *8* (5), 937–947. https://doi.org/10.1021/acssynbio.9b00034.

(12) Noireaux, V.; Libchaber, A. A Vesicle Bioreactor as a Step toward an Artificial Cell Assembly. *Proc. Natl. Acad. Sci.* **2004**, *101* (51), 17669–17674. https://doi.org/10.1073/pnas.0408236101.

(13) Shin-ichiro M. Nomura; Kanta Tsumoto; Tsuomu Hamada; Kazunari Akiyoshi; Yoichi Nakatani; Kanichi Yoshikawa. Gene Expression within Cell-Sized Lipid Vesicles. *ChemBioChem* **2003**, *4*, 1172–1175.

(14) Kurihara, K.; Tamura, M.; Shohda, K.; Toyota, T.; Suzuki, K.; Sugawara, T. Self-Reproduction of Supramolecular Giant Vesicles Combined with the Amplification of Encapsulated DNA. *Nat. Chem.* **2011**, *3* (10), 775–781. https://doi.org/10.1038/nchem.1127.

(15) Bagatolli, L. A.; Gratton, E. Two Photon Fluorescence Microscopy of Coexisting Lipid Domains in Giant Unilamellar Vesicles of Binary Phospholipid Mixtures. *Biophys. J.* **2000**, *78* (1), 290–305. https://doi.org/10.1016/S0006-3495(00)76592-1.

(16) Zhao, J.; Wu, J.; Heberle, F. A.; Mills, T. T.; Klawitter, P.; Huang, G.; Costanza, G.; Feigenson, G. W. Phase Studies of Model Biomembranes: Complex Behavior of DSPC/DOPC/Cholesterol. *Biochim. Biophys. Acta BBA - Biomembr.* **2007**, *1768* (11), 2764–2776. https://doi.org/10.1016/j.bbamem.2007.07.008.

(17) Zhao, J.; Wu, J.; Shao, H.; Kong, F.; Jain, N.; Hunt, G.; Feigenson, G. Phase Studies of Model Biomembranes: Macroscopic Coexistence of Lα+Lβ, with Light-Induced Coexistence of Lα+Lo Phases. *Biochim. Biophys. Acta BBA - Biomembr.* **2007**, *1768* (11), 2777–2786. https://doi.org/10.1016/j.bbamem.2007.07.009.

(18) Konyakhina, T. M.; Goh, S. L.; Amazon, J.; Heberle, F. A.; Wu, J.; Feigenson, G. W. Control of a Nanoscopic-to-Macroscopic Transition: Modulated Phases in Four-Component DSPC/DOPC/POPC/Chol Giant Unilamellar Vesicles. *Biophys. J.* **2011**, *101* (2), L8–L10. https://doi.org/10.1016/j.bpj.2011.06.019.

(19) Herold, C.; Chwastek, G.; Schwille, P.; Petrov, E. P. Efficient Electroformation of Supergiant Unilamellar Vesicles Containing Cationic Lipids on ITO-Coated Electrodes. *Langmuir* **2012**, *28* (13), 5518–5521. https://doi.org/10.1021/la3005807.

(20) Reeves, J. P.; Dowben, R. M. Formation and Properties of Thin-Walled Phospholipid Vesicles. *J. Cell. Physiol.* **1969**, *73* (1), 49–60. https://doi.org/10.1002/jcp.1040730108.

(21) Darszon, A.; Vandenberg, C. A.; Schönfeld, M.; Ellisman, M. H.; Spitzer, N. C.; Montal, M. Reassembly of Protein-Lipid Complexes into Large Bilayer Vesicles: Perspectives for Membrane Reconstitution. *Proc. Natl. Acad. Sci.* **1980**, *77* (1), 239–243. https://doi.org/10.1073/pnas.77.1.239.

(22) Needham, D.; McIntosh, T. J.; Evans, E. Thermomechanical and Transition Properties of Dimyristoylphosphatidylcholine/Cholesterol Bilayers. *Biochemistry* **1988**, *27* (13), 4668–4673. https://doi.org/10.1021/bi00413a013.

(23) Angelova, M. I.; Dimitrov, D. S. Liposome Electroformation. 13.

(24) Dimitrov, D. S.; Angelova, M. I. Lipid Swelling and Liposome Formation Mediated by Electric Fields. 14.

(25) Dimitrov, D. S.; Angelova, M. I. Lipid Swelling and Liposome Formation on Solid Surfaces in External Electric Fields. In *New Trends in Colloid Science*; Hoffmann, H., Ed.; Progress in Colloid & Polymer Science; Steinkopff: Darmstadt, 1987; Vol. 73, pp 48–56. https://doi.org/10.1007/3-798-50724-4_62.

(26) Boban, Z.; Mardešić, I.; Subczynski, W. K.; Raguz, M. Giant Unilamellar Vesicle Electroformation: What to Use, What to

Avoid, and How to Quantify the Results. *Membranes* **2021**, *11* (11), 860. https://doi.org/10.3390/membranes11110860.
(27) Pott, T.; Bouvrais, H.; Méléard, P. Giant Unilamellar Vesicle Formation under Physiologically Relevant Conditions. *Chem. Phys. Lipids* **2008**, *154* (2), 115–119. https://doi.org/10.1016/j.chemphyslip.2008.03.008.
(28) Drabik, D.; Doskocz, J.; Przybyło, M. Effects of Electroformation Protocol Parameters on Quality of Homogeneous GUV Populations. *Chem. Phys. Lipids* **2018**, *212*, 88–95. https://doi.org/10.1016/j.chemphyslip.2018.01.001.
(29) Groves, J. T. Bending Mechanics and Molecular Organization in Biological Membranes. *Annu. Rev. Phys. Chem.* **2007**, *58* (1), 697–717. https://doi.org/10.1146/annurev.physchem.56.092503.141216.
(30) Rozovsky, S.; Kaizuka, Y.; Groves, J. T. Formation and Spatio-Temporal Evolution of Periodic Structures in Lipid Bilayers. *J. Am. Chem. Soc.* **2005**, *127* (1), 36–37. https://doi.org/10.1021/ja046300o.
(31) Rodriguez, N.; Pincet, F.; Cribier, S. Giant Vesicles Formed by Gentle Hydration and Electroformation: A Comparison by Fluorescence Microscopy. *Colloids Surf. B Biointerfaces* **2005**, *42* (2), 125–130. https://doi.org/10.1016/j.colsurfb.2005.01.010.
(32) Faizi, H. A.; Tsui, A.; Dimova, R.; Vlahovska, P. M. Bending Rigidity, Capacitance, and Shear Viscosity of Giant Vesicle Membranes Prepared by Spontaneous Swelling, Electroformation, Gel-Assisted, and Phase Transfer Methods: A Comparative Study. *Langmuir* **2022**, *38* (34), 10548–10557. https://doi.org/10.1021/acs.langmuir.2c01402.
(33) Hauri, E. H.; Papineau, D.; Wang, J.; Hillion, F. High-Precision Analysis of Multiple Sulfur Isotopes Using NanoSIMS. *Chem. Geol.* **2016**, *420*, 148–161. https://doi.org/10.1016/j.chemgeo.2015.11.013.
(34) Kraft, M. L. Phase Separation of Lipid Membranes Analyzed with High-Resolution Secondary Ion Mass Spectrometry. *Science* **2006**, *313* (5795), 1948–1951. https://doi.org/10.1126/science.1130279.
(35) Boxer, S. G.; Kraft, M. L.; Weber, P. K. Advances in Imaging Secondary Ion Mass Spectrometry for Biological Samples. *Annu. Rev. Biophys.* **2009**, *38* (1), 53–74. https://doi.org/10.1146/annurev.biophys.050708.133634.
(36) Grusky, D. S.; Moss, F. R.; Boxer, S. G. Recombination between ^{13}C and ^{2}H to Form Acetylide ($^{13}C_2{}^2H^-$) Probes Nanoscale Interactions in Lipid Bilayers via Dynamic Secondary Ion Mass Spectrometry: Cholesterol and GM_1 Clustering. *Anal. Chem.* **2022**, *94* (27), 9750–9757. https://doi.org/10.1021/acs.analchem.2c01336.
(37) Lozano, M. M.; Hovis, J. S.; Moss, F. R.; Boxer, S. G. Dynamic Reorganization and Correlation among Lipid Raft Components. *J. Am. Chem. Soc.* **2016**, *138* (31), 9996–10001. https://doi.org/10.1021/jacs.6b05540.
(38) Larsen, J.; Hatzakis, N. S.; Stamou, D. Observation of Inhomogeneity in the Lipid Composition of Individual Nanoscale Liposomes. *J. Am. Chem. Soc.* **2011**, *133* (28), 10685–10687. https://doi.org/10.1021/ja203984j.
(39) Moss, F. R.; Boxer, S. G. Atomic Recombination in Dynamic Secondary Ion Mass Spectrometry Probes Distance in Lipid Assemblies: A Nanometer Chemical Ruler. *J. Am. Chem. Soc.* **2016**, *138* (51), 16737–16744. https://doi.org/10.1021/jacs.6b10655.
(40) Kahya, N.; Scherfeld, D.; Bacia, K.; Poolman, B.; Schwille, P. Probing Lipid Mobility of Raft-Exhibiting Model Membranes by Fluorescence Correlation Spectroscopy. *J. Biol. Chem.* **2003**, *278* (30), 28109–28115. https://doi.org/10.1074/jbc.M302969200.
(41) Konyakhina, T. M.; Feigenson, G. W. Phase Diagram of a Polyunsaturated Lipid Mixture: Brain Sphingomyelin/1-Stearoyl-2-Docosahexaenoyl-Sn-Glycero-3-Phosphocholine/Cholesterol. *Biochim. Biophys. Acta BBA - Biomembr.* **2016**, *1858* (1), 153–161. https://doi.org/10.1016/j.bbamem.2015.10.016.
(42) Boban, Z.; Mardešić, I.; Subczynski, W. K.; Jozić, D.; Raguz, M. Optimization of Giant Unilamellar Vesicle Electroformation for Phosphatidylcholine/Sphingomyelin/Cholesterol Ternary Mixtures. *Membranes* **2022**, *12* (5), 525. https://doi.org/10.3390/membranes12050525.